OPTIMAL FREQUENCY SELECTION FOR DESIGNING A SUPERCONDUCTING RIM-DRIVEN PROPULSION MOTOR

A. Hassannia **A. Darabi**
Faculty of Electrical and Robotic Engineering, University of Shahrood
Shahrood, 316-3619995161, Iran, Email: amir.hassannia@gmail.com

M.E. Ghazi
Faculty of Physics, University of Shahrood
Shahrood, 316-3619995161, Iran

***Abstract**: Electrical propulsion systems have been developed in marine transportation in recent decades. Generally, an electric propulsion system consists of an induction, permanent magnet or conventional synchronous motor that is supplied by a DC batteries set and inverter-based drive system. Therefore, the working frequency of the propulsion motor and drive system can be considered as an arbitrary parameter. This paper deals with selecting the best rated frequency to minimize the losses of a superconducting rim-driven propulsion system. Several loss components of a case study motor are analyzed in rather wide-range of possible rated frequencies. The optimum frequency for designing the case study motor is then determined, and the motor is redesigned. Comparing the main performance characteristics of the new motor and original one shows a considerable decrement in total losses of the propulsion motor and drive system.*

***Key words:** Superconductivity, Synchronous motor, Rim-driven propulsion, Design optimization.*

1. Introduction

Marine electrical propulsion systems have been improved greatly in recent years [1-3]. Various types of electrical motors have been developed for azimuth, podded, and rim-driven propulsion systems. The rim-driven propulsion system has attracted much attention due to the superior advantages in efficiency and better hydrodynamic performance [4]. The radial thickness (stator outer radius mines rotor inner radius) of the rim-driven motor is an important parameter in this type of propulsion system. This parameter forms the surface that is directly in contact with the water flow. The radial thichness should be decreased as much as possible in order to decreasing the drag loss and improving the hydrodynamic performance of propulsion system[5].

On the other hand, the technology of superconductivity has extended greatly in many industries [6-7]. High temperature superconducting (HTS) motors have advantages in compactness and more efficiency, which have extended their applications in marine electrical propulsion systems [8-9]. Various types of superconducting motors have been designed and build for azimuth and podded thrusters. Unfortunately, the air-gap, and consequently, the radial thickness of superconducting machines are rather big, which limits the application of HTS motors in the rim-driven marine propulsion systems. Recently, few works have been reported, dealing with the design of enough thin superconducting motors for rim-driven applications [10]. This new system is very appealing due to the combination of the advantages of superconducting motors and rim-driven propulsion system simultaneously.

The conceptual structure of a typicall marine propulsion system is shown in Fig. 1. The propulsion motor is supplied by a DC batteries set and a DC to AC switch-mode inverter.

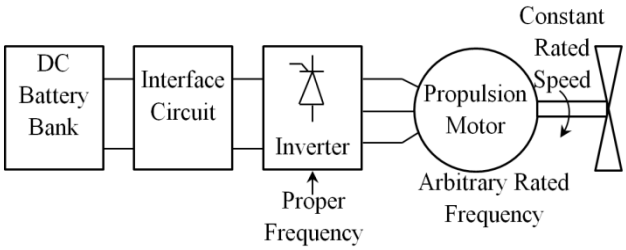

Fig. 1. Conceptual structure of marine propulsion system.

The inverter output voltage and frequency must be the same as motor-rated voltage and frequency, while both of them are arbitrary parameters. Rated voltage of the propulsion motor is usually selected as the maximum possible value. The rated frequency Selection needs more care. Rated frequency of the propulsion system has a significant influence on different components of system losses such as motor core loss, motor winding loss, and inverter switching loss. Furthermore, rated speed of the propulsion motor is considered as a constant parameter that is given by the propeller rated speed. Therefore, the number of poles of the propulsion motor is changed in different frequencies to keep the speed constant. As a consequence, the propulsion motor radial thickness, and consequently, the hydraulic loss are affected by the rated frequency. However, selecting a proper frequency in order to minimize the total loss of propulsion system is an important issue that has not yet been investigated in details.

Design optimization of electrical motors has been discussed in many papers [11-12]. The present paper deals with selecting the optimal frequency for designing a HTS rim-driven propulsion system. A recently designed 2.5 MW HTS rim-driven motor is selected as case study [10]. Various optimal designs of the selected motor are presented for a set of different rated frequencies. The main-loss components are evaluated, and the optimal rated frequency is selected via a trade-off.

2. Case study machine

A HTS salient-pole synchronous motor is selected as the case study machine, which has been designed recently for a rim-driven propulsion system [10]. The motor consists of an ordinary stator and a cored rotor with HTS field winding. Figure 2 shows a general scheme of the machine structure, and a 3D-view of the main parts of the designed machine is illustrated in Fig. 3. The main parameters of this machine are shown in Table 1.

The design algorithm of HTS rim-driven motors machine has been described in [10], which can be repeated for different rated frequencies. Some difficulties of this process are deal with by selecting the proper values for arbitrary design parameters such as electrical loading factor (ac) and air-gap flux density (B_{ag}) in different frequencies. Another problem is calculating the constant factors such as leakage flux factor, which is usually determined through a trial and error procedure. This method is absurdly time-consuming especially when the design procedure should be repeated for a set of different frequencies. In this regard, an analytical formulation of the leakage flux factor is essential.

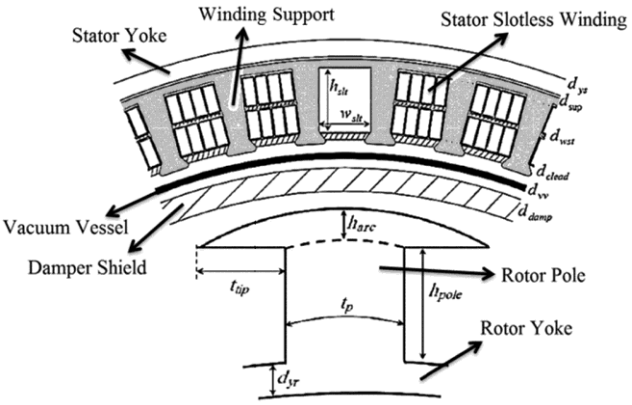

Fig. 2. An overview of selected structure.

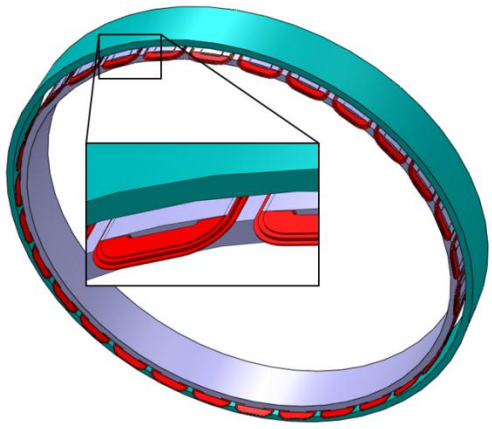

Fig. 3. Main parts of case study machine.

Table 1. Design parameters of case study motor.

Parameters	Values	Units
Rated power	2.5	MW
Effective line voltage	400	V
Frequency	55	Hz
Rated speed	220	rpm
Rotor inner diameter	3000	mm
Maximum axial length	600	mm
Maximum radial thickness	165	mm

3. Analytical calculation of leakage flux factor

Leakage flux factor is an essential parameter in the design process, which explains the normalized rotor leakage flux as:

$$k_{leak} = 1 - \frac{\varphi_{st}}{\varphi_r} \tag{1}$$

where φ_{st} and φ_r are the fluxes that are passing from the cross-section of the stator and rotor yoke respectively. Many researchers have tried to derive an analytic formulation for calculation of this parameter [13-14]. They have developed proper equivalent circuits for different structures of electrical machines. For each structure, few approximate equations have been presented considering the equivalent circuit. These equations are not applicable for the thin and exceptional structure of rim-driven machines. Therefore, we considered a simple equivalent circuit for the rim-driven machines, as shown in Fig. 4. According to the proposed circuit, the leakage flux factor can be defined as:

$$k_{leak} = \frac{\Re_1 \Re_3 + 2\Re_2 \Re_3}{\Re_1 \Re_2 + \Re_1 \Re_3 + 2\Re_2 \Re_3} \tag{2}$$

in which the air-gap reluctances are approximated for the thin structure of this machine as:

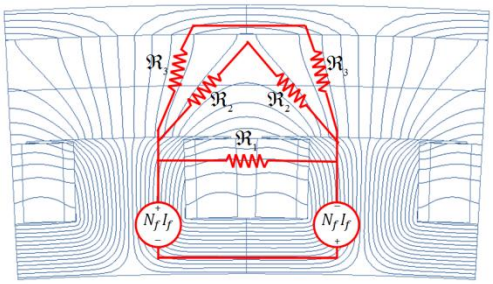

Fig. 4. Magnetic equivalent circuit of rim-driven machine.

$$\Re_1 = \frac{1}{\mu_0 \cdot L} \times \frac{R_{or} y_p - t_p}{0.9 \times h_{pole}} \tag{3}$$

$$\Re_2 = \frac{1}{\mu_0 \cdot L} \times \frac{\sqrt{\left(R_{or} y_p - t_p\right)^2 + Ag^2}}{Ag} \tag{4}$$

$$\Re_3 = \frac{1}{\mu_0 \cdot L} \times \frac{1.1 \times Ag}{\frac{t_p}{2.5} + \frac{R_{or} y_p}{2.1}} \tag{5}$$

where R_{or} is outer radius of rotor, y_p is pole pitch angle, t_p is wide of rotor pole body, h_{pole} is pole height, Ag is air-gap, and L is axial length of stator core. The results of (2) were compared with those obtained from FE simulation for few different designs of rim-driven motor, and all show good agreement. These comparisons are not illustrated here for conciseness.

4. Design in different rated frequencies

The relation between rated frequency, rated speed (n_r), and numbers of rotor poles (p) is as follows:

$$n_r = \frac{120\, f}{p} \tag{6}$$

The rated speed is constant, according to Table 1. Since the numbers of rotor poles is an even integer variable, there are several discrete possible values for rated frequency. We considered a set of rated frequencies as integer coefficients of 11 in the range of 22 Hz to 418 Hz. For each individual frequency, a recently developed design algorithm for HTS rim-driven machines [10] that is shown in Fig. 5, was applied to redesign the case study motor.

The values of air-gap flux density and electrical loading factor should be properly selected for each individual frequency. The weight and volume of the machine are decreased when air-gap flux density is increased. Any increment in the air-gap flux density needs extra field winding. Due to the space limitation between rotor poles in the rim-driven machines, the extra field winding increases the rotor pole height. The leakage flux factor is increased by the pole height increment. Therefore, more field winding is needed in order to compensate the increased leakage flux, which leads to more increment of the rotor pole

height. This loop is usually diverged if the air-gap flux density is increased above a critical value. There is always a maximum accessible value of air-gap flux density in each frequency. Some previously works have reported similar results for the maximum air-gap flux density [15].

However, selecting a proper value for the air-gap flux density needs more care. Many simulations show that besides decreasing the volume and axial length of the machine, the radial thickness is increased by any increment of the air-gap flux density [10]. In fact, the superconducting rim-driven motor design problem involves a rather complicated trade-off between compactness and radial thickness minimization. It is accepted that the design algorithm of HTS rim-driven motors should be started with a relatively low value of air-gap flux density, and its value is then increased gradually until the value of axial length becomes less than a maximum pre-defined value [10]. The electrical loading factor is adjusted for each value of the air-gap flux density according to Fig. 5. Figure 6 shows the optimum and maximum accessible values of air-gap flux density for each individual frequency.

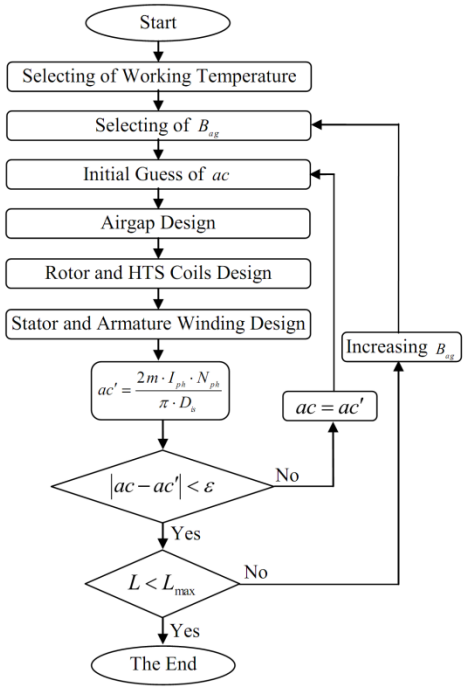

Fig. 5. General chart of design algorithm.

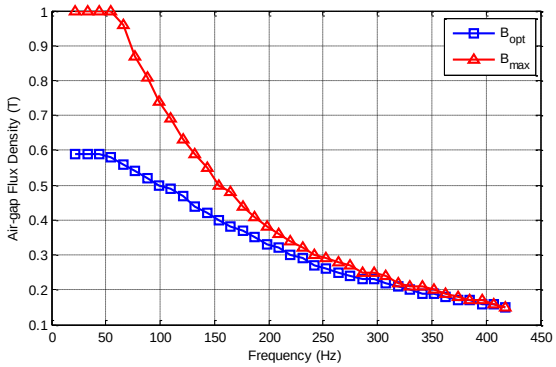

Fig. 6. Optimum and maximum accessible values of air-gap flux density for each frequency.

There is a critical point at which the optimum frequency cuts the maximum one. Above this point, the maximum accessible air-gap flux density is less than the optimum frequency, and consequently, the motor axial length will exceed its maximum pre-defined value. Figure 7 shows the optimal design results obtained for the axial length and radial thickness of the case study motor in each frequency.

However, one can decrease the radial thickness of the rim-driven motor by frequency increment below the critical frequency. As a consequence, the drag force and hydraulic loss of the rim-driven propulsion system decrease in higher frequencies. The hydraulic loss should be calculated for each value of radial thickness in order to be able to compare to the other components of system losses. The optimum rated frequency is determined via a trade-off between different-loss components of the propulsion system.

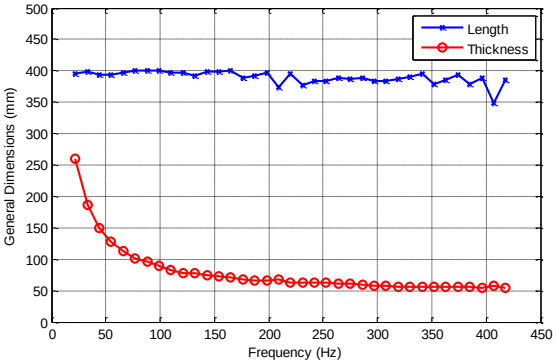

Fig. 7. Axial length and radial thickness of the machine related to optimum air-gap flux density.

5. Frequency-dependent losses

5.1. Hydraulic loss

The water drag force on the rim-driven motor can be calculated using Eq. 7 [16],

$$F_d = \frac{1}{2}\rho V^2 C_d A \tag{7}$$

where ρ is fluid density, V is object velocity, and A is cross-sectional area of the object on a plane perpendicular to the direction of motion. Parameter C_d (drag coefficient) is a function of Reynolds number, which characterizes the flow as:

$$\mathrm{Re} = \frac{V D}{\nu} \tag{8}$$

where D denotes the characteristic length, and ν is the kinematic viscosity. The relations between C_d and Re are given in fluids handbooks for different shapes [16-17]. For the ring-shape of the rim-driven motor, the drag coefficient is $C_d \approx 1.2$ when the Reynolds number is bigger than 1000 [17]. Therefore, considering the average typical velocity of submarines as $V = 4\,\mathrm{m/s}$, the drag force can be calculated for each design of the HTS rim-driven case study motor. The drag loss is then calculated as:

$$P_{drg} = F_d V \tag{9}$$

Figure 8 shows how the drag loss is decreased with the rated frequency increment.

5.2. Stator core loss

The stator core material of the case study machine is selected among more conventional laminated electrical steels (65JN1600).

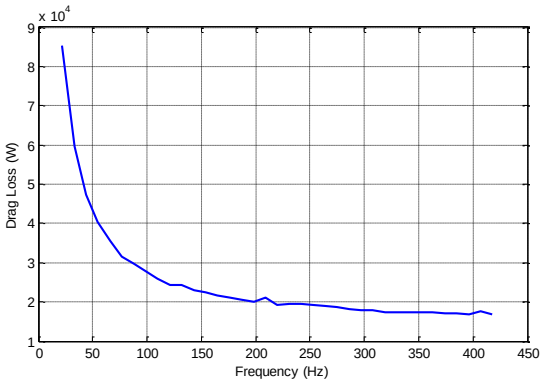

Fig. 8. Drag loss vs. rated frequency.

According to the datasheet, the core loss density of selected material is a function of the working frequency and maximum flux density of the stator core, as shown in Fig. 9.

The maximum flux density of the stator is a coefficient of the air-gap flux density, which is changed with the rated frequency according to Fig. 6. Considering the set of rated frequencies and related maximum flux densities of the stator, the stator core loss density can be calculated using the data in Fig. 9. The stator core volume and maximum flux density are decreased with frequency increment. Therefore, the stator core loss is increased due to the frequency increment, and is decreased due to the decrement of the stator core volume and maximum flux density. As a consequence, the stator core loss of the case study machine is fluctuated with frequency increment, as shown in Fig. 10.

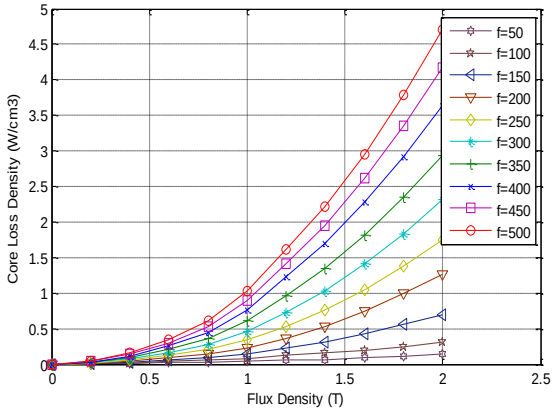

Fig. 9. Core loss density as a function of frequency and maximum flux density.

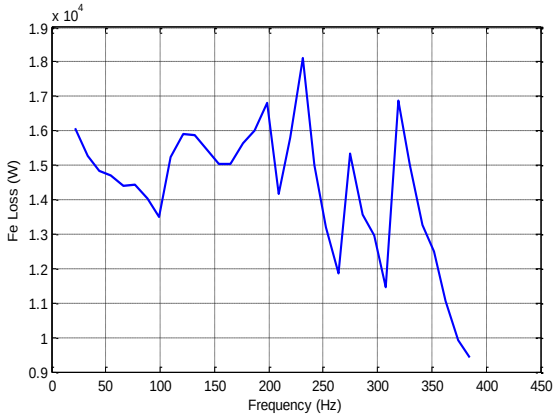

Fig. 10. Stator core loss versus rated frequency.

5.3. Stator winding loss

The skin effect is affected by frequency variation, which changes the resistance of copper winding. Skin depth is a function of frequency as follow [18]:

$$\delta = \frac{1}{\sqrt{\pi \mu f \sigma}} \tag{10}$$

where σ and μ are resistivity and magnetic permeability of copper, respectively. The skin depth varies between 14 and 3.2 mm when the frequency changes from 22 to 418 Hz. Since the skin depth is extremely bigger than the diameter of the stator's copper-wire, the stator winding resistance and stator winding loss are not changed considerably due to the skin effect.

5.4. Switching loss of drive system

Typical propulsion motors are supplied by variable frequency inverter and DC batteries bank (a set of interconnected batteries). The inverter contains several switches that are turned on and off continuously. As intuitively expected, the switches do not have ideal characteristics. Once a switch is turned on, the current build up consists of a raise time, and the voltage falls to zero with a down time. Large values of the switch current and switch voltage occur simultaneously during the on or off transition. Therefore, energy is dissipated during transitions. The average switching power loss of a switch due to the on and off transitions is written as [19]:

$$P_s = \frac{1}{2} V_d I_d f_s \left(t_{on} + t_{off}\right) \tag{11}$$

where V_d and I_d are voltage and current of DC side, respectively, f_s is switching frequency, and t_{on} and t_{off} are on and off transition times, respectively. Switching frequency is a coefficient of the inverter output frequency. This coefficient (frequency modulation ratio) is defined as:

$$m_f = \frac{f_s}{f} \tag{12}$$

Equation (11) shows that the switching power loss varies linearly with the switching frequency. In the motor drive applications, the triangular wave-form signal and the control signal of the PWM inverter should be synchronized to each other to avoid the undesired sub-harmonics [19]. This implies that the frequency modulation ratio is an odd integer, usually greater than 21 [19]. Therefore, the switching frequency, and consequently, the switching power loss are increased linearly by the motor rated frequency increment. Assuming a typical three-phase synchronous PWM inverter including 9 thyristor switches, Figure 11 shows how the switching loss changes with the rated frequency.

6. Optimal design of propulsion motor

Drag loss, stator core loss, and switching loss are the three important components of the propulsion system loss that are changed with the rated frequency. An optimal design of the propulsion motor can be obtained, in which the total loss of the propulsion system is minimized. Figure 12 shows the sum of drag loss, stator core loss, and switching loss of the propulsion system for the selected set of rated frequencies. This figure shows that the minimum loss occurs when the rated frequency is 99 Hz.

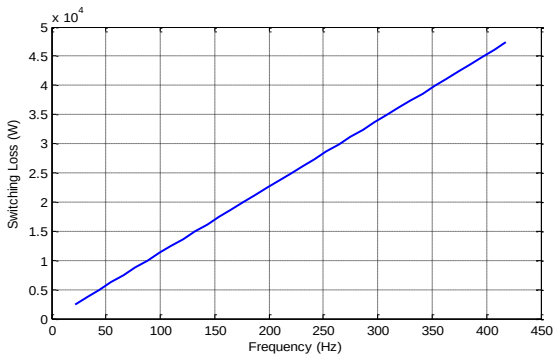

Fig. 11. Switching loss vs. rated frequency.

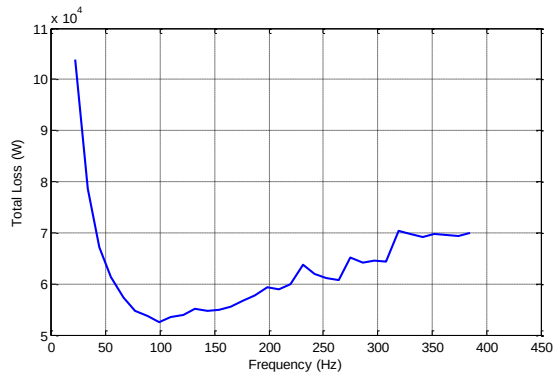

Fig. 12. Total loss of the machine vs. rated frequency.

The mentioned design algorithm of HTS rim-driven machines was applied to redesign the case study motor at the new rated frequency (99 Hz). Some design parameters and performance characteristics of the newly designed motor and original one [10] are compared in Table 2. The comparison shows some advantages of the newly designed motor in efficiency, size, and weight.

Furthermore, the correctness of the design algorithm and analytical formulations were investigated using the finite elements method (FEM). A 2D FE model of a pairs of poles of the machine was developed to calculate the flux density distribution in no-load condition, as shown in Fig. 13. The FEM results obtained for the flux densities of different parts of the machine show good agreement with the values estimated during the design procedure.

Table 2. Comparison of optimized design of case study motor and original one.

Parameters	Original design	Optimized design	Unit
Rated power	2.5	2.5	MW
Effective line voltage	400	400	V
Rated speed	220	220	rpm
Rated frequency	55	99	Hz
Air-gap flux density	0.65	0.5	T
Leakage flux factor	0.027	0.2	-
Axial length	363	400	mm
Radial thickness	150.5	89.5	mm
Volume of active parts	0.5407	0.3404	m^3
Drag loss	47581	27748	W
Core loss	17197	13495	W
Switching loss	6229	11212	W
Sum of frequency dependent losses	71007	52455	W

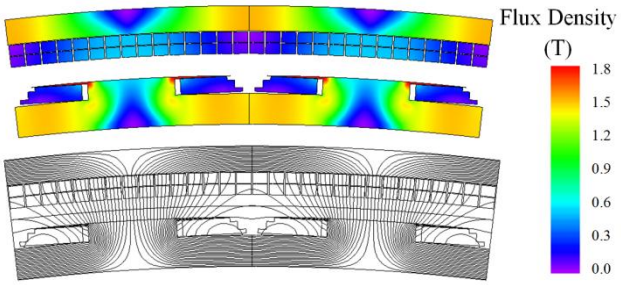

Fig. 13. Flux lines and flux density distribution in no-load condition.

The FE model was then utilized to calculate the fluxes that are passing from the stator and rotor yoke, as shown in Fig. 14. Now the leakage flux factor can be calculated as:

$$k_{leak} = 1 - \frac{\varphi_{st}}{\varphi_r} = 1 - \frac{0.0112}{0.0139} = 0.194 \qquad (13)$$

which shows good agreement with the value of $k_{leak} \approx 0.2007$ that was estimated using the proposed analytical formula in section 3.

Load condition performance and some other characteristics such as the maximum flux density on HTS coils and stator core loss were investigated using the FEM, not illustrated here for conciseness.

7. Conclusion

The inverter-based supplying of the propulsion motors provides the possibility of designing the propulsion system with different rated frequencies. Various types of losses that occur in propulsion motor and drive system are affected by rated frequency. The optimum rated frequency for designing the 2.5 MW case-study propulsion motor was obtained by trade-off between different losses of the system as 99 Hz. The motor was redesigned with optimum rated frequency, and was analyzed using FEM, which shows significant improvement in the machine performance characteristics. For the case-study machine, the sum of hydraulic loss, stator core loss, and switching loss is decreased by %26 by optimum selection of the rated frequency.

Acknowledgement

The authors would like to thank the Research Center of Electric Propulsions, University of Shahrood, and the Marine Industry Organization for their support and information.

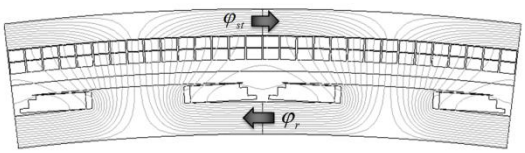

Fig. 14. Surfaces that indicate the flux passing from stator and rotor yoke.

References

1. Gieras, J.F.: *Advancements in Electric Machines*, Springer, Rockford, Illinois, U.S.A., 2008.
2. Mccoy, T.J., Amy J.V.: *The state-of-the-art of integrated electric power and propulsion systems and technologies on ships.* In: Proceedings of the IEEE Electric Ship Technologies Symposium, 2009, Baltimore, MD, p. 340–344. Doi:10.1109/ESTS.2009.4906534
3. Yutao, C., Fanming, Z., Jiaming, W.: *Integrated Design Platform for Marine Electric Propulsion System*. In: Energy Procedia, Part A, (2012), Vol. 17, p. 540-546.
4. Yakovlev, A.Y., Sokolov, M.A., Marinich N.V.: *Numerical design and experimental verification of a rim-driven thruster*. In: Proceedings of the Second International Symposium on Marine Propulsors, 2011, Hamburg, Germany.
5. Sharkh, S.M., Lai, S.H.: *Slotless PM Brushless Motor With Helical Edge-Wound Laminations*. In: IEEE Transactions on Energy Conversion, (2009), Vol. 21, No. 3, p. 594-598.
6. Tixador, P.: *Development of superconducting power devices in Europe*. In: Physica C 470, (2010), p. 971–979.
7. Fang, Y.T, Gao, C.Y, Yao Y.Y, 2005. *Design and analysis of superconducting magnets of a new mixed Maglev model.* In: Journal of Zhejiang University of Science A (Applied Physics & Engineering), (2005), Vol. 6, No. 7, p. 716-721. Doi:10.1631/jzus.2005.A0716
8. Gamble, B., Snitchler, G., MacDonald, T.: *Full Power Test of a 36.5 MW HTS Propulsion Motor*. In: IEEE Transactions on Applied Superconductivity, (2011), Vol. 21, No. 3, p. 1083-1088.
9. Li, J., Chau, K.T.: *A Novel HTS PM Vernier Motor for Direct-Drive Propulsion.* In: IEEE Transactions on Applied Superconductivity, (2011), Vol. 21, No. 3, p. 1175-1179.
10. Hassannia, A., Darabi, A.: *Design and Performance Analysis of Superconducting Rim-Driven Synchronous Motors for Marine Propulsion*. In: IEEE Transactions on Applied Superconductivity, (2014), Vol. 24, No. 1, Doi: 10.1109/TASC.2013.2280346
11. Faiz, J., Sharifian, M.B.: *Optimal design of three phase induction motors and their comparison with a typical industrial motor.* In: Computers & Electrical Engineering, (2001), Vol. 27, No. 2, p. 133–144. Doi:10.1016/S0045-7906(00)00010-0
12. Tudorache, T., Popescu, M.: *Optimal design solutions for permanent magnet synchronous machines.* In: Advances in Electrical and Computer Engineering Journal, (2011), Vol. 11, No. 4, p. 77-82. Doi:10.4316/aece.2011.04012
13. Hwang, C.C., Chang, S.M., Pan, C.T., Chang, T.Y.: *Estimation of parameters of interior permanent magnet synchronous motors.* Journal of Magnetism and Magnetic Materials, (2002), Vol. 239, p. 600–603. Doi:10.1016/S0304-8853(01)00647-3
14. Meessen, K.J., Thelin, P., Soulard, J., Lomonova, E.A.: *Inductance calculations of permanent-magnet synchronous machines including flux change and self and cross saturations.* In: IEEE Transactions on Magnets, (2008), Vol. 44, p. 2324-2331. Doi:10.1109/TMAG.2008.2001419
15. Gieras, J.F., Wang, R.J., Kamper, M.J.: *Axial Flux Permanent Magnet Brushless Machines*, Kluwer Academic Publishers, New York, 2005. ISBN: 1-4020-2661-7.
16. Young, D.F., Bruce, R.M., Theodore, H.O., Wade, W.H.: *A Brief Introduction to Fluid Mechanics, fourth edition*, John Wiley and Sons, Hoboken, 2007.
17. Janna, W.S.: *Introduction to Fluid Mechanics, fourth edition*, Taylor & Francis Group, 1993. ISBN: 1420085247.
18. Kim, H.M., Yoon, Y.S., Kwon, Y.K., Kim, Y.C., Lee, S.H., Hong, J.P., Song, J.B., Lee, H.G.: *Design of damper to protect the field coil of an HTS synchronous motor.* In: IEEE Transactions on Applied Superconductivity, (2009), Vol. 19, p. 1683-1686. Doi:10.1109/TASC.2009.2017842
19. Mohan, N., Undeland, T.M., Robbins, W.P.: *Power Electronics: Converters, Applications, and Design*. Third edition, John Wiley and Sons, New York, 2002. ISBN: 0471226939.

Authors' Information

Amir Hassannia was born in Gonabad, Iran, on February 1984. He received the B.Sc. degree from the Ferdowsi University of Mashhad, Mashhad, Iran, in 2006, and the M.Sc. degree from the Faculty of Electrical and Robotic Engineering, University of Shahrood, Shahrood, Iran, in 2008, both in electrical engineering. He is currently working toward the Ph.D. degree in the same university. His research interests include design and modeling of electrical machines, new superconducting motors and fuzzy control.

Ahmad Darabi received the B.S. degree in electrical engineering from Tehran University, Tehran, Iran in 1989 and the M.S. degree in the same field from Ferdowsi University of Mashhad, Mashhad, Iran, in 1992. He obtained the Ph.D. degree with the electrical machine group, Queen's University, Belfast, UK, in 2002. He is now with the Faculty of Electrical and Robotic Engineering, University of Shahrood, Shahrood, Iran. His research activities are mostly on design, modeling and manufacturing of miniature electrical machines and generating sets.

Mohammad Ebrahim Ghazi is an associate professor and works with Faculty of Physics, University of Shahrood, Shahrood, Iran.